

EFFECTS OF OPTICALLY SHALLOW BOTTOMS ON WATER-LEAVING RADIANCES

Curtis D. Mobley and Lydia Sundman

Sequoia Scientific, Inc.

15317 NE 90th Street

Redmond, WA 98052 USA

mobley@sequoiasci.com phone: 425-867-2464 ext 109 fax: 425-867-5506

Hao Zhang and Kenneth J. Voss

Department of Physics

University of Miami

Coral Gables, FL 33124 USA

Optically shallow bottoms affect the reflected, upwelling radiance in various ways. The magnitude and angular distribution of the bottom-reflected radiance are determined by the bidirectional reflectance distribution function (BRDF) of the bottom. If the bottom is inhomogeneous, or patchy, the upwelling radiance is a spatial function of horizontal location as well as depth, and therefore three-dimensional (3D) radiative transfer (RT) calculations are necessary to predict the in-water and water-leaving radiances. Similarly, if the bottom is not level, 3D radiative transfer calculations are necessary.

Because of the great computational expense of doing 3D RT calculations—as opposed to using a 1D RT model that assumes a horizontally homogeneous, level bottom—it is important to quantify the errors that result from using a 1D model when a 3D model should be used. Likewise, it is almost always assumed that bottom BRDFs are Lambertian, when in reality all materials are non-Lambertian reflectors. Again, the errors resulting from the assumption of a Lambertian BRDF need to be quantified.

In the present paper we restrict ourselves to situations that are relevant to remote sensing of the oceans by the PHILLS (Portable Hyperspectral Imaging Low Light Spectrometer) airborne sensor, which is being used extensively in the CoBOP (Coastal Benthic Optical Properties) and HyCODE (Hyperspectral Coastal Ocean Dynamics Experiment) field programs. This application restricts the solar and reflected (viewing) angles to a limited range of values. Remote sensing with PHILLS is usually performed when the solar zenith angle is ~45 deg, and PHILLS views the ocean at nadir angles from 0 to 30 deg and at an azimuthal angle perpendicular to the sun's direction. A solar angle of 45 deg corresponds to an in-water incident angle of ~32 deg for the sun's direct beam incident on the bottom (for a level sea surface and no scattering within the water), and an in-air nadir viewing angle of 30 degrees corresponds to light reflected from the bottom at an in-water angle of ~22 deg. Thus the water-leaving radiance is affected by the BRDF over its full range of incident and reflected angles only to the extent that multiple scattering within the water adds to the radiance of the unscattered direct solar beam as reflected into the viewing direction. Likewise, 3D “edge effects” near boundaries between patches of different bottom material arise from multiple scattering within the water column.

BRDF EFFECTS

We first consider the effects of non-Lambertian BRDFs for homogeneous, level bottoms. A BRDF is a function of four angles: the incident polar and azimuthal angles (θ_i, φ_i) and the reflected angles (θ_r, φ_r). A Lambertian BRDF is independent of these angles: $\text{BRDF}_{\text{Lamb}}(\theta_i, \varphi_i, \theta_r, \varphi_r) = \rho/\pi$, where ρ is the reflectivity of the surface. For a Lambertian surface (only), the irradiance reflectance of the surface, $R = E_r/E_d$, is independent of the incident radiance, and $R = \rho$. Actual surfaces such as sand or plant canopies have BRDFs that depend on the incident and reflected angles, and which often show features such as retroreflection (“hot spots”) and specular reflection. Figure 1 shows a BRDF measured on white, ooid sand near Lee Stocking Island, Bahamas. The incident angle is $(\theta_i, \varphi_i) = (35,0)$, and the plot shows the BRDF as a function of reflected angles (θ_r, φ_r) for the discrete angles at which the BRDF was measured (blue lines). This sand shows noticeable retroreflection [the peak near $(\theta_r, \varphi_r) = (35,0)$], but no specular reflection. The red lines in the figure are an analytic function fit to the data (Voss *et al.*, 2000). The literature contains many empirical formulas for the BRDFs of terrestrial vegetation such as grasslands, crops, and forest canopies (e.g., Cabot and Dedieu, 1997). Figure 2 shows, for example, a wheatfield BRDF for an incident angle of $(\theta_i, \varphi_i) = (40,0)$ (Rahman, *et al.*, 1993). The BRDFs of aquatic vegetation such as seagrass beds have yet to be measured.

To study the effects of non-Lambertian BRDFs on water-leaving radiances, we used analytical fits to BRDF measurements for sand (Fig. 1) and other bare substrates (Voss *et al.*, 2000), and we used various analytical formulas for terrestrial vegetation canopies (wheat, clover, lawngrass, coniferous forest) as ersatz seagrass BRDFs. These BRDFs were used to define the bottom boundary conditions for radiative transfer simulations using the Hydrolight 4.1 radiative transfer model (www.sequoiasci.com/hydrolight.html). The water absorption and scattering properties (IOPs), incident sky radiance, and bottom depth were varied over a range of conditions appropriate to remote sensing situations. Figure 3 illustrates the results for one particular simulation, defined as follows:

- water IOPs characteristic of clear Bahamas water at 480 nm (total $a = 0.054 \text{ m}^{-1}$, $b = 0.284 \text{ m}^{-1}$, Petzold phase function)

- sun at 60 deg in a clear sky

- wind speed of 5 m/s

- bottom depth, 1 m

- wheatfield (ersatz seagrass) BRDF vs. Lambertian BRDF with the same R

The shallow depth and clear water used in this simulation mean that the bottom BRDF (rather than the water column) largely determines the water-leaving radiance L_w ; the solar zenith angle of 60 deg accentuates any effects due to the nonLambertian nature of the bottom. For these conditions, $R = 0.058$ for the non-Lambertian bottom. The irradiance reflectance of a non-Lambertian BRDF depends on the incident lighting, i.e. on the solar angle, water depth, and IOPs in the oceanic environment. However, for this BRDF, the value of R varies by less than 2 percent as the solar angle varies from 0 to 60 degrees and the water depth varies from 1 to 30 m.

Figure 3 shows the percent errors that result in the water-leaving radiance L_w if the non-Lambertian (wheatfield) BRDF is replaced by a Lambertian BRDF of the same reflectance R . The maximum error of -20 percent near the viewing direction $(\theta_v, \phi_v) = (60, 180)$ occurs where the hot spot gives increased L_w values, i.e., replacing the non-Lambertian BRDF with a Lambertian BRDF gives 20 percent too little L_w at the hot spot direction. However, the angles relevant to PHILLS remote sensing are viewing directions at right angles to the sun and from the nadir out to 30 deg; these angles are within the green box in Fig. 3. For the PHILLS remote sensing angles, the Lambertian L_w is within 4 percent of the correct value even for this very shallow bottom. This error decreases as the water depth increases or the solar angle decreases.

Simulations with a variety of non-Lambertian BRDFs (not shown here) show that a non-Lambertian bottom BRDF can be replaced by a Lambertian BRDF having the same irradiance reflectance R , with errors of no more than 10 percent in the water-leaving radiance, for viewing directions relevant to PHILLS remote sensing. Note that the percentage errors can be larger for other viewing directions, and the errors in the upwelling radiance as measured underwater, near the bottom, can be much larger, especially at nearly horizontal viewing angles.

A BACKWARD MONTE CARLO 3D RT MODEL

If the bottom is non-homogeneous or sloping, there are effects in the upwelling radiance that require a 3D RT model for investigation. Such a code, called BMC3D, was developed using backward Monte Carlo ray tracing techniques as described in Gordon (1985). The BMC3D code can simulate bottoms whose BRDF depends arbitrarily on location, and the bottom can slope uniformly in one direction. The water-column IOPs are assumed to be uniform. The incident sky radiance can be arbitrary (BMC3D uses the same sky radiance model as Hydrolight). The sea surface is modeled by capillary waves. A simulated sensor can be placed at any (x, y, z) location in the water, with any nominal viewing direction (θ_v, ϕ_v) , and having any angular response function (for computation of plane and scalar irradiances or radiance, including a delta-function response for idealized radiance calculations). The code is computationally efficient because all generated photon packets contribute to the estimated radiance or irradiance.

EDGE EFFECTS FOR PATCHY BOTTOMS

Let us next consider a large, uniform, dark seagrass patch with $R = 0.05$ next to a large, uniform, bright sand patch with $R = 0.5$. Suppose we tow a Tethered Spectral Radiometer Buoy (TSRB; www.satlantic.com) across the seagrass-sand boundary and measure L_u at depth $z = 0.7$ m beneath the sea surface as a function of position x across the boundary. This is illustrated in Fig. 4, where the grass is the region for $x < 0$ and the sand is the region for $x \geq 0$. As the TSRB goes from the middle of the grass to the middle of the sand, L_u will go from a value for an all-grass bottom to a value for an all-sand bottom (each of which can be computed by a 1D model). There will be a grass-to-sand transition region near the edge, where the TSRB “sees” parts of each bottom type; this

transition depends on the sensor response function. Multiple scattering within the water column also makes light reflected from one bottom type appear to come from the other bottom type, as illustrated in Fig. 4. This multiple scattering is a 3D effect that depends on the water IOPs.

We can isolate how much of the L_u “edge blurring” is due to sensor response and how much is due to multiple scattering by comparing simulations using an actual TSRB response function (both effects) with simulations using a delta-function sensor response (multiple-scattering effects only). Figure 5 shows the results of one series of simulations, which used the same water IOPs as for the BRDF simulations described above. The water depth was 5 m, and the grass and sand bottoms both had Lambertian BRDFs with their respective reflectances. A measured angular response function was used for the TSRB (the nominal field of view (FOV) is ~ 10 deg half width at half max). The TSRB measures L_u at a depth of 0.7 m. For this distance of 4.3 m above the bottom, the nominal FOV sees a circle on the bottom of radius 0.76 m.

In Fig. 5, the green lines show L_u as predicted by the 1D Hydrolight model, which must treat the bottom as either all grass or all sand. The red points in Fig. 5 show the $L_u(x)$ values as computed by the BMC3D code, using the actual TSRB FOV response function. For the 10^6 photon packets traced in each Monte Carlo simulation, the BMC3D values are within two percent of the Hydrolight values when the bottom is uniform, or at large distances (> 5 m) from the boundary. We see that the TSRB begins to be affected by the boundary at about 2 m from the boundary. The blue points show BMC3D simulations of $L_u(x)$ as would be measured by an idealized radiometer with a δ -function (perfectly collimated) response. The edge effects in these simulations are due only to multiple scattering within the water column, since the sensor “sees” a point on the bottom. The purple line is $L_u(x)$ as predicted by a simple model (discussed below) based on the 1D solution and the actual TSRB sensor response.

Regarding the simulated TSRB values as correct, Fig. 6 shows the errors that would result from using the other (Hydrolight, δ -function, or model) values in place of the correct TSRB values. The percent error is defined as $100[L_u(\text{other}) - L_u(\text{TSRB})]/L_u(\text{TSRB})$; a positive (negative) error means that the other estimate is larger (smaller) than the correct value.

As expected, the 1D (Hydrolight) solution is inadequate near the grass-sand boundary; the errors can be almost a factor of two in this simulation. However, if the difference between the 1D and 3D solutions is due primarily to sensor-response effects rather than to true 3D, multiple-scattering effects, then it should be possible to approximate $L_u(x)$ with a simple model that weights the 1D grass/sand solutions according to how much of the grass/sand bottom is seen by the sensor. This model is defined by

$$L_u(x; \text{model}) = \frac{\int \int L_u(x', y'; 1D) S[\alpha(x', y')] dx' dy'}{\int \int S[\alpha(x', y')] dx' dy'}. \quad (1)$$

Here (x',y') is a point on the bottom in a coordinate system centered on the sensor (x,y) position; $L_u(x',y';1D)$ is either the grass or the sand 1D (Hydrolight) solution, and $S[\alpha(x',y')]$ is the TSRB sensor response for off-axis angle α as determined by the sensor location and the bottom point. The purple line in Fig. 5 shows the values of $L_u(x)$ as predicted by this model. Figure 6 shows that this model gives agreement with the actual TSRB $L_u(x)$ values to within 25 percent, which is much better than the 1D solution alone. Thus we see that a simple 1D RT model combined with a sensor response model can give a greatly improved prediction of the true 3D radiance. However, if errors of less than ~25% (for the conditions of this particular simulation) are required in L_u near the boundary, then a 3D RT calculation must be performed.

EFFECTS OF SLOPING BOTTOMS

Three-dimensional effects also occur if the bottom is not horizontal, as illustrated in Fig. 7. The upwelling radiance will now depend on the bottom slope θ_b and on the sun's azimuthal angle φ_s . A prediction of L_u therefore requires a 3D radiative transfer code.

A series of BMC3D runs was made for different bottom slopes and solar zenith and azimuthal angles, using the water IOPs and other input as in the simulations discussed above. The water depth directly below the L_u sensor was 5 m. The bottom was modeled as a Lambertian BRDF with a reflectivity of 0.5, as is reasonable for sand. We also ran Hydrolight with the same input and a level bottom at depth 5 m. The solid lines in Fig. 8 shows the errors in L_u that occur for a solar angle of $\theta_s = 45$ deg if the correct 3D (BMC3D) calculation is replaced by a 1D, constant-depth (Hydrolight) calculation, using the nominal 5 m depth of the water just below the sensor. The curves are color-coded and labeled by the azimuthal angle φ_s ($\varphi_s = 0$ means the sun is in the "downslope" direction). The figure shows that the difference in the exact 3D and approximate 1D L_u values is ~10 percent for bottom slopes of 10 deg; the error can be many tens of percent for larger bottom slopes.

L_u depends on θ_b and φ_s primarily through the change in the incident angle θ_i (measured relative to the normal to the bottom) of the unscattered solar beam onto the bottom. This angle is given by

$$\cos\theta_i = \sin\theta_b \sin\theta_{sw} \cos\varphi_s + \cos\theta_b \cos\theta_{sw}, \quad (2)$$

where θ_{sw} is the in-water solar zenith angle (relative to the z axis), obtained from θ_s and Snell's law. By definition of the BRDF, $L_u = BRDF \cdot E_{\perp} \cdot \cos\theta_i$. Thus a simple model for L_u that adjusts the 1D (level bottom, Lambertian BRDF) solution by an incident-angle factor is

$$L_u(3D) = L_u(1D) \cos\theta_i / \cos\theta_{sw}. \quad (3)$$

The dashed lines in Fig. 8 show that the errors between the exact BMC3D values and the values given by the 1D (Hydrolight) solution and the simple model of Eqs. (2) and (3) are

less than 5 percent for a bottom slope of 10 deg and are ~10 percent for bottom slopes of ~20 deg. Thus, for gently sloping bottoms with $\theta_b < 10$ deg, a 1D RT model can be used with a correction factor (Eq. 3) to predict L_u with better than 5% accuracy. A full 3D RT calculation must be done for steeply sloping bottoms or if more accuracy is required.

CONCLUSIONS

The simulations shown here were chosen to show several “worse-case” situations for shallow, very clear waters. Even in such situations, the errors in water-leaving radiances resulting from the assumption of a Lambertian BRDF are generally less than 10 percent for geometries relevant to PHILLS remote sensing. If a 1D RT model is used instead of a 3D RT model, errors in near-surface, upwelling radiances can be tens of percent near highly contrasting, sharp boundaries and for bottoms with slopes of more than 10 degrees from the horizontal. However, simple modifications of the 1D solutions can reduce these errors considerably and may make them tolerable in light of the other errors in remote sensing simulations—such as atmospheric correction effects—and the high computational costs of performing 3D RT simulations instead of 1D simulations. The errors shown above are smaller in many instances (e.g., optically deeper bottoms or less contrast between bottom reflectances). Full 3D RT simulations must be used for predictions of bottom-reflected radiances near the bottom or at nearly horizontal viewing directions.

ACKNOWLEDGMENTS

This work was supported by the Coastal Benthic Optical Properties (CoBOP) Program of the U. S. Navy Office of Naval Research. Emmanuel Boss of Oregon State University supplied the ac-9 IOP measurements used in the simulations of Bahamas waters. Scott McLean of Satlantic supplied the measured TSRB response function.

REFERENCES

- Cabot, F. and G. Dedieu, 1997. Surface albedo from space: Coupling bidirectional models and remotely sensed measurements, *J. Geophys. Res.* 102(D16), 19645-19663.
- Gordon, H. R., 1985. Ship perturbation of irradiance measurements at sea. 1: Monte Carlo simulations, *Appl. Optics* 24(23), 4172-4182.
- Rahman, H., B. Pinty, and M. M. Verstraete, 1993. Coupled surface-atmosphere reflectance (CSAR) model. 2. Semiempirical surface model usable with NOAA AVHRR data. *J. Geophys. Res.*, 98(D11), 20791-20801.
- Voss, K. J., H. Zhang, and A. Chapin, 2000. Bi-directional reflectance distribution functions (BRDF) of benthic surfaces in the littoral zone. Ocean Optics XV extended abstract (this volume).

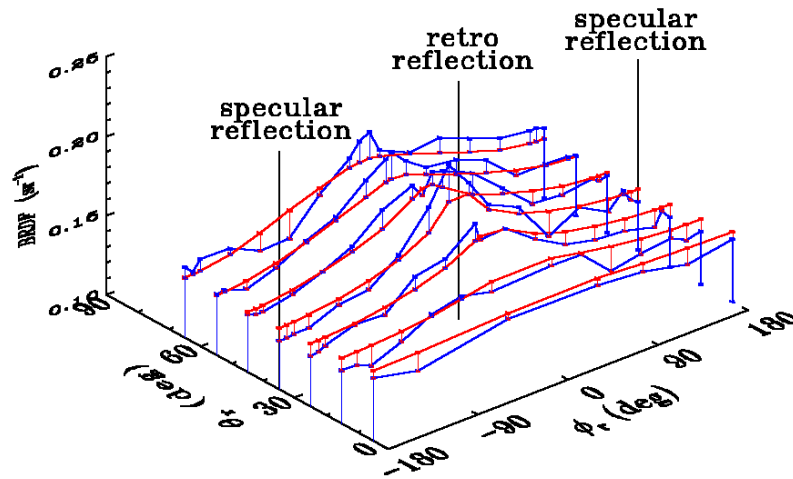


Fig. 1. Example of a measured BRDF for ooid sand at Lee Stocking Island, Bahamas. The incident angle is $(\theta_i, \phi_i) = (35, 0)$; the wavelength is 479 nm. The directions corresponding to retro- and specular reflection are labeled. Blue lines are measured data; red lines are an analytic function fit to the data.

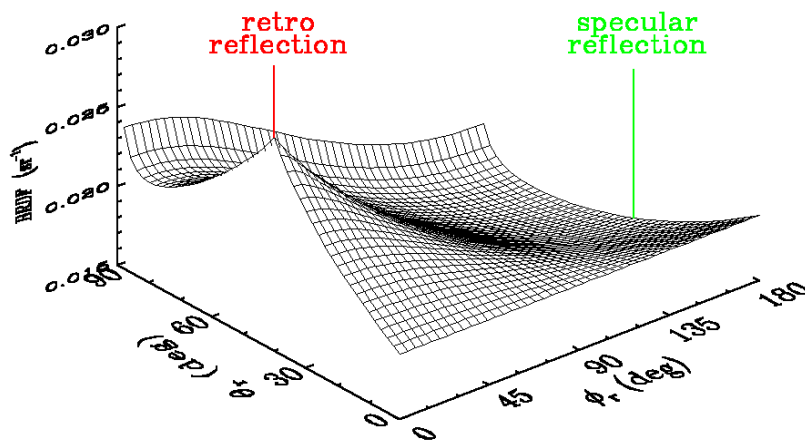


Fig. 2. An analytic function fit to the BRDF of a wheatfield for an incident angle of $(\theta_i, \phi_i) = (40, 0)$.

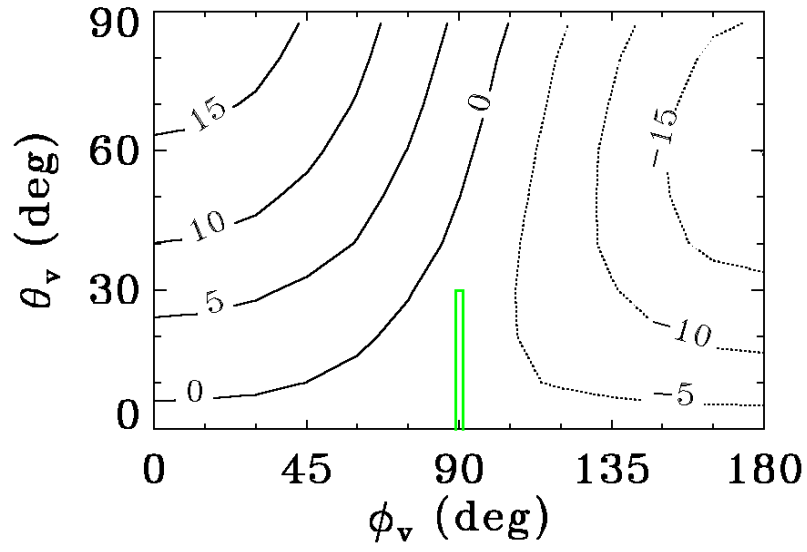


Fig. 3. Percent errors in water-leaving radiance when the non-Lambertian BRDF of Fig. 2 is replaced by a Lambertian BRDF having the same reflectance R , for a bottom depth of 1 m and IOPs as described in the text. The green box bounds the nominal angles relevant to remote sensing by the PHILLS airborne sensor.

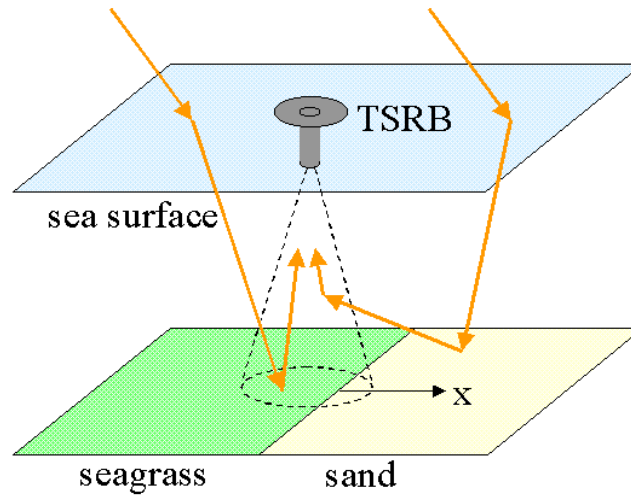


Fig. 4. Illustration of sensor field-of-view and multiple-scattering effects near a seagrass-sand bottom boundary.

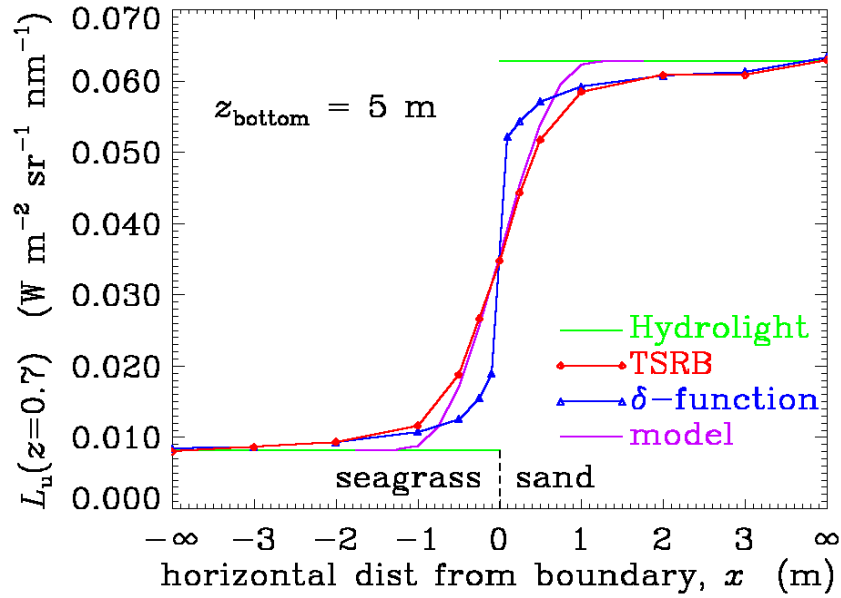


Fig. 5. Comparison of upwelling radiances as computed by Hydrolight, by the BMC3D code using the measured TSRB sensor response and using a δ -function response, and using the Hydrolight solution in the model of Eq. (1).

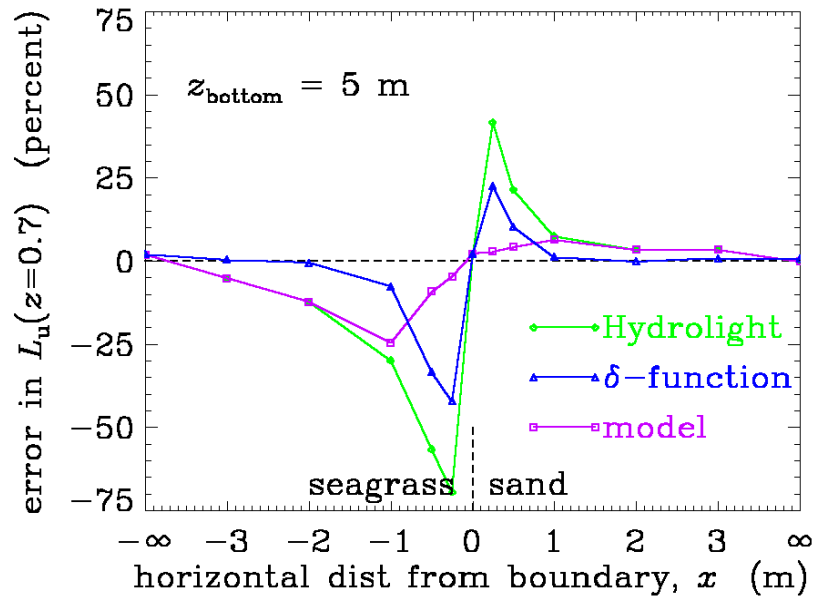


Fig. 6. Errors between the TSRB radiances of Fig. 5 and those computed in other ways.

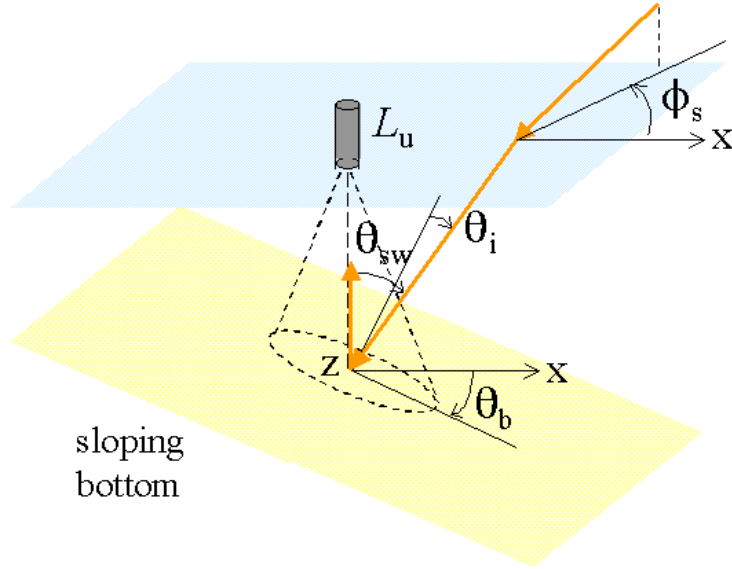


Fig. 7. Illustration of a sloping bottom. θ_b is the angle of the bottom slope relative to the +x (downslope) direction; ϕ_s is the azimuthal angle of the sun relative to +x; θ_{sw} is relative to +z; and θ_i is relative to the normal to the bottom.

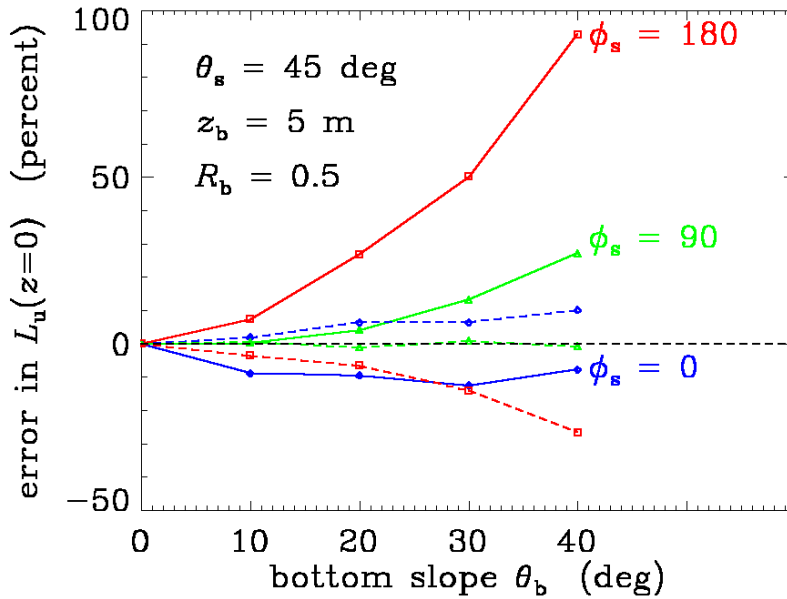


Fig. 8. Errors in L_u just beneath the sea surface that result if the exact 3D, sloping-bottom RT calculation is replaced by a 1D calculation using a level bottom (solid lines), and the errors resulting when the 1D solution is modified by the model of Eq. (3) (dashed lines).